8-21-2013

Photoisomerization and Photoinduced Reactions in Liquid CCl4 and CHCl3

Scott Reid
Marquette University, scott.reid@marquette.edu

Fawzi Abou-Chahine
University of Bristol

Thomas J. Preston
University of Bristol

Greg T. Dunning
University of Bristol

Andrew J. Orr-Ewing
University of Bristol

See next page for additional authors

Journal of Physical Chemistry : A, Vol. 117, No. 50 (December 19, 2013): 13388–13398. DOI.

Photoisomerization and Photoinduced Reactions in Liquid CCl_4 and $CHCl_3$

Fawzi Abou-Chahine
School of Chemistry, University of Bristol, Cantock's Close, Bristol BS8 1TS, U.K.
Thomas J. Preston
School of Chemistry, University of Bristol, Cantock's Close, Bristol BS8 1TS, U.K.
Greg T. Dunning
School of Chemistry, University of Bristol, Cantock's Close, Bristol BS8 1TS, U.K.
Andrew J. Orr-Ewing
School of Chemistry, University of Bristol, Cantock's Close, Bristol BS8 1TS, U.K.
Gregory M. Greetham
Central Laser Facility, Research Complex at Harwell, Science and Technology Facilities Council, Rutherford Appleton Laboratory, Harwell Science and Innovation Campus, Didcot, Oxfordshire, OX11 0QX, U.K.
Ian P. Clark

Central Laser Facility, Research Complex at Harwell, Science and Technology Facilities Council, Rutherford Appleton Laboratory, Harwell Science and Innovation Campus, Didcot, Oxfordshire, OX11 0QX, U.K.

Mike Towrie

Central Laser Facility, Research Complex at Harwell, Science and Technology Facilities Council, Rutherford Appleton Laboratory, Harwell Science and Innovation Campus, Didcot, Oxfordshire, OX11 0QX, U.K.

Scott A. Reid

Department of Chemistry, Marquette University, 535 North 14th Street, Milwaukee, Wisconsin 53233, United States

Abstract

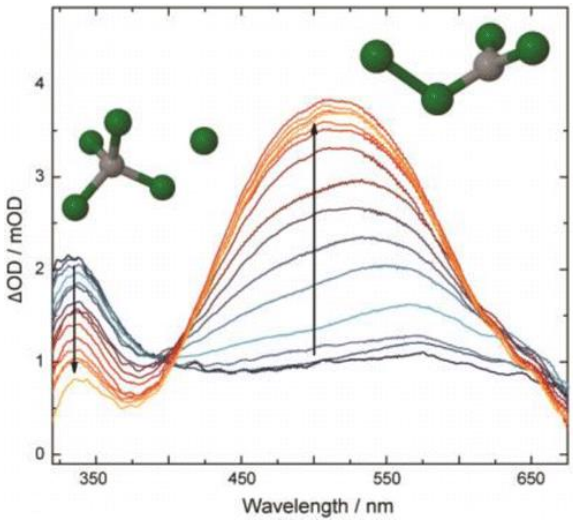

Transient absorption spectroscopy is used to follow the reactive intermediates involved in the first steps in the photochemistry initiated by ultraviolet (266-nm wavelength) excitation of solutions of 1,5-hexadiene, isoprene, and 2,3-dimethylbut-2-ene in carbon tetrachloride or chloroform. Ultraviolet and visible bands centered close to 330 and 500 nm in both solvents are assigned respectively to a charge transfer band of Cl-solvent complexes and the strong absorption band of a higher energy isomeric form of the solvent molecules (*iso*-CCl_3–Cl or *iso*-$CHCl_2$–Cl). These assignments are supported by calculations of electronic excitation energies. The isomeric forms have significant contributions to their structures from charge-separated resonance forms and offer a reinterpretation of previous assignments of the carriers of the visible bands that were based on pulsed radiolysis experiments. Kinetic analysis demonstrates that the isomeric forms are produced *via* the Cl–solvent complexes. Addition of the unsaturated hydrocarbons provides a reactive loss channel for the Cl–solvent complexes, and reaction radii and bimolecular rate coefficients are derived from analysis using a Smoluchowski theory model. For reactions of Cl with 1,5-hexadiene, isoprene, and 2,3-dimethylbut-2-ene in CCl_4, rate coefficients at 294 K are, respectively, $(8.6 \pm 0.8) \times 10^9$, $(9.5 \pm 1.6) \times 10^9$, and $(1.7 \pm 0.1) \times 10^{10}$ M^{-1} s^{-1}. The larger reaction radius and rate coefficient for 2,3-dimethylbut-2-ene are interpreted as evidence for an H-atom abstraction channel that competes effectively with the channel involving addition of a Cl-atom to a C═C bond. However, the addition mechanism appears to dominate the reactions of 1,5-hexadiene and isoprene. Two-photon excited CCl_4 or $CHCl_3$ can also ionize the diene or alkene solute.

SPECIAL ISSUE

This article is part of the Terry A. Miller Festschrift special issue.

1 Introduction

The kinetics and dynamics of reactions of chlorine atoms with organic molecules in the gas phase have been the subject of extensive experimental and theoretical investigation.(1, 2) For reactions with alkanes, H-atom abstraction occurs via a direct mechanism, either over a low energy barrier or *via* a barrierless process, and the reaction typically produces HCl that is vibrationally and rotationally cold. However, reactions of Cl-atoms with unsaturated hydrocarbons exhibit addition pathways that compete with or can dominate the direct abstraction pathway.(3-9) The energized adduct may eliminate HCl under low pressure conditions, but at ambient pressures of a few Torr or more, collisional stabilization of the adduct can become favorable,(10) with implications for atmospheric reaction pathways. The HCl may be produced vibrationally excited for unusually exothermic reactions of Cl-atoms with alkenes such as propene, in which the H-atom abstraction pathway forms a resonance-stabilized allyl radical.(3)

For free radical chlorination reactions in solution, Cl-atom complexes with the solvent play an important mechanistic role,(11, 12) and reactions of such complexes with various solutes are emerging as model systems for studying chemical kinetics and dynamics in organic solvents. For example, Hochstrasser and co-workers(13) and Crim and co-workers(14) used ultrafast transient infrared (IR) absorption spectroscopy to follow the time dependence of the production of HCl from reactions of Cl-atoms with alkanes. Crim and co-workers(14-16) also used a charge-transfer band in the ultraviolet (UV) region, previously assigned to Cl–solvent complexes,(17, 18) to follow the reaction kinetics on picosecond to nanosecond time scales, and applied this approach to reactions of Cl-atoms with alkanes, alcohols, and chloroalkanes. More recently, we monitored the HCl products of reactions of Cl-atoms with 2,3-dimethylbut-2-ene in CCl_4 or $CDCl_3$ solutions using ultrafast transient IR absorption spectroscopy and observed that 15–25% of the HCl is initially formed vibrationally excited in this exothermic abstraction reaction.(19) Addition of a Cl-atom followed by solvent stabilization of the adduct might be expected to dominate such reactions of unsaturated solutes, based on observations of the pressure dependence of the mechanisms of related gas-phase reactions. However, the reaction of Cl-atoms with 2,3-dimethylbut-2-ene demonstrates that abstraction pathways can compete.

In the current work, we explore further the reactions of Cl-atoms with unsaturated hydrocarbons in solution, using either CCl_4 or $CHCl_3$ as the solvent and as a photolytic source of Cl-atoms. We adopt the method of Crim and co-workers(14-16) to follow the kinetics of reactions using the near-UV charge-transfer bands characteristic of Cl-atoms in these solvents. By probing the reaction products using a white-light continuum (WLC) spanning the near-UV and visible regions of the spectrum, we also observe the time evolution of a second spectral feature centered in the visible region that is a signature of another transient species in the solutions. The source of this visible band, which is also known from radiolysis experiments in CCl_4, has been the subject of prior debate. However, assignments derived from radiolysis and UV photolysis have converged to a solvent separated ion pair, denoted here by $CCl_3^+\|Cl^-$,(20-22) or a charge-transfer complex $CCl_3^{\delta+}$–$Cl^{\delta-}$,(23) although the mechanisms of formation are suggested to differ for the two excitation methods. On the basis of evidence from the observed kinetics of growth of the spectral band, and with the support of electronic structure calculations, we propose an assignment to an isomeric form of CCl_4, denoted by *iso*-CCl_3–Cl. In chloroform, the visible band is assigned to the corresponding *iso*-$CHCl_2$–Cl species. Our assignments are similar in spirit to the earlier literature, but more consistent with recent experimental and computational studies of other halogenated methanes such as bromoform ($CHBr_3$).(24-26) Iso species of this type are important as reactive agents in solution: for example, prior calculations indicated that *iso*-CH_2X–X (X = Cl, Br, I) species are the methylene transfer agents that produce cyclopropane in reactions of UV photoexcited CH_2X_2 with ethene.(27, 28) This cyclopropane production is

accompanied by X_2 loss in a one-step process, and in the case of X = Cl, the barrier to reaction was computed to be 37 kJ mol^{-1}.

The alkenes we study here are 1,5-hexadiene, isoprene (2-methyl-1,3-butadiene), and 2,3-dimethylbut-2-ene, but to extract quantitative information for the rates and mechanisms of their reactions, spectroscopic measurements of the UV-induced photochemistry of the pure solvents, CCl_4 and $CHCl_3$, are also required. Time-resolved electronic absorption spectra of CCl_4 and $CHCl_3$ photoproducts are therefore presented and analyzed to provide a framework for the photochemistry in the alkene solutions. We also undertook time-resolved vibrational spectroscopy studies of all the solutions, but these were less informative than the electronic spectroscopy data, with the exception of the 2,3-dimethylbut-2-ene system which was the focus of an earlier publication.(19) The transient spectral features observed in infrared absorption measurements for 1,5-hexadiene can all be assigned to radical cation pathways.(29)

2 Experimental and Computational Details

2.1 Transient Electronic Absorption Spectroscopy

Transient UV and visible absorption spectra were obtained using the ULTRA Laser Facility at the STFC Rutherford Appleton Laboratory, and full details of the laser system have been presented elsewhere.(30) A titanium:sapphire oscillator (Femtolaser) generated pulses of 800 nm wavelength light at a 65 MHz repetition rate which pumped a regenerative amplifier (Thales Optronique) operating at 10 kHz. The amplifier emitted ≤1 mJ pulses centered at 800 nm and of the duration 40–80 fs. Third harmonic generation (THG) produced pulses of 266-nm light, and the current experiments typically used 1 μJ of this UV radiation. Focusing <10 μJ of the 800 nm output from the amplifier into a rastered 2-mm thick CaF_2 window generated a probe WLC which spanned wavelengths over the range 300–750 nm. After passage through the sample, the WLC was dispersed onto a 512-element silicon array (Quantum Detectors) to obtain UV–visible absorption spectra. A portion of the WLC bypassed the sample and was dispersed onto a second, equivalent array to provide a reference spectrum. However, for most of the results presented here, the reference spectrum was not required for data processing. Spectra were wavelength-calibrated using a series of narrow band-pass filters. The spectra were not corrected for the temporal chirp in the WLC: instead, data for time delays ≤1 ps were excluded from analysis.

The pump-pulse train was chopped at 5 kHz to facilitate collection of pump on–pump off difference spectra. The relative linear polarizations of the pump and probe pulses were set to the magic angle 54.7°. Spectra were obtained at about 50 selected, but randomly ordered, time delays between pump and probe pulses in the range 1–2000 ps. These delays were controlled using a motorized delay stage (Newport IMS600LM) on the pump beam path.

A peristaltic pump circulated samples through a Harrick cell fitted with CaF_2 windows spaced by 0.35 mm. The position of the cell was rastered in a plane perpendicular to the laser propagation direction, and the flow rate was chosen to ensure that successive laser pulses probed fresh portions of the sample. The samples probed were CCl_4, $CHCl_3$ (both solvents >99% purity, Sigma Aldrich), $CDCl_3$ (Sigma Aldrich, >99.96 atom % D), and 0.25–0.75 M solutions of 1,5-hexadiene (97%, Sigma Aldrich), isoprene (≥99%, Sigma Aldrich), or 2,3-dimethylbut-2-ene (Sigma Aldrich, >99.9%) in these chlorinated solvents. Samples were dried using molecular sieves (4 Å) prior to use, and all glassware was stored in a drying oven between experiments. Measurements were made at an ambient temperature of 294 K.

2.2 Calculations of Molecular Structures and Spectra

Electronic structure calculations used the Gaussian 09 software package(31) on the Marquette University (MU) Pere high speed cluster. Full geometry optimizations were carried out using density functional theory (DFT) (with the meta-GGA hybrid functional M06-2X)(32) and post-Hartree–Fock (MP2) methods with an aug-cc-pVTZ basis

set, either in vacuum or in neat solvent. Calculations in solvent used the Polarizable Continuum Model (PCM) as implemented in Gaussian 09. Characterization of the isomerization reaction coordinates started from relaxed redundant C–Cl–Cl bond angle scans. Structures corresponding to the energy maxima on these scans were then optimized as first-order saddle points, and intrinsic reaction coordinate (IRC) calculations were performed to verify that these saddle points correspond to transition states on the isomerization path. For the radical complexes, optimization used the same methods, with counterpoise correction for basis set superposition error (BSSE). All calculated binding energies were also corrected for zero-point energy. Natural Bond Orbital (NBO) calculations(33, 34) were carried out on the MU Pere cluster with NBO Version 5.9.(35)

Electronic spectra were calculated with time-dependent DFT (TDDFT) methods using the M06-2X and CAM-B3LYP(36, 37) functionals, with an aug-cc-pVTZ basis set. The performance of the M06-2X method has recently been benchmarked for electronic excitations, including Rydberg and charge-transfer transitions.(38) TDDFT calculations in solvent also used the PCM method.

3 Results and Discussion

Measurements were made of transient absorption in the near-UV and visible regions for 266-nm photoexcited samples of CCl_4 and $CHCl_3$ (and $CDCl_3$), and for dilute solutions of selected unsaturated hydrocarbons (1,5-hexadiene, isoprene, and 2,3-dimethylbut-2-ene) in these chlorinated solvents. Results are presented first for the neat solvents, with analysis using a kinetic scheme based on the Smoluchowski model employed by Crim and co-workers for Cl-atom reactions in solution.(14-16) This analysis is then applied to the kinetics of reactions taking place in solutions containing the unsaturated hydrocarbons.

3.1 Photoinduced Complexation and Isomerization in CCl_4 and $CHCl_3$

Figure 1 shows the time evolution of the transient electronic absorption bands observed upon UV excitation of neat CCl_4 and $CHCl_3$ and recorded using the procedures described in section 2. One relatively sharp and short-lived band, centered near 330 nm, and a second, long-lived, and very broad band centered close to 500 nm appear in CCl_4. These features were previously observed in experiments on picosecond and nanosecond time scales(18, 20-23) and, in the case of photolytic production at 266 nm, shown to derive from two-photon excitation of the solvent. Hereafter, these two bands will be referred to as the 330-nm (or UV) and 500-nm (or visible) features. Figure 1 also shows time-resolved spectra for $CHCl_3$, and similar bands are observed centered at about the same wavelengths. $CDCl_3$ displayed almost identical behavior to $CHCl_3$.

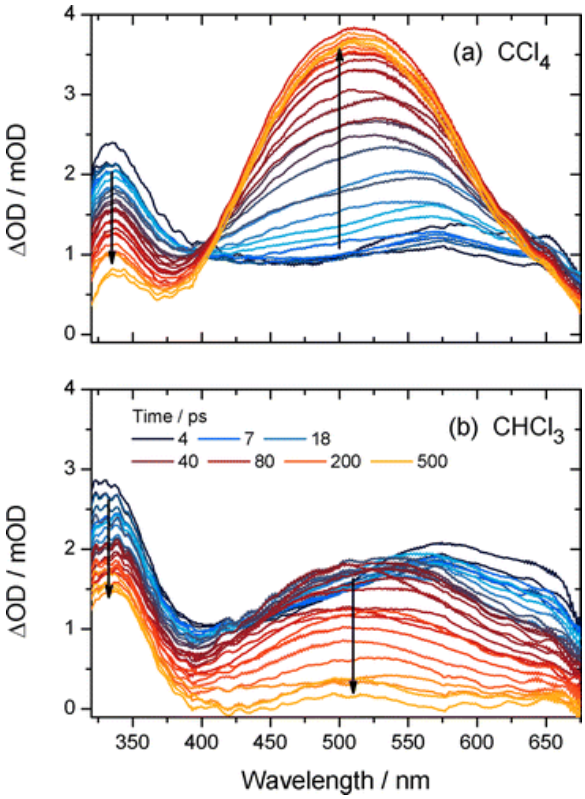

Figure 1. Time-resolved transient absorption spectra obtained following photoexcitation at 266 nm of samples of (a) CCl_4 and (b) $CHCl_3$. The inset key shows selected time delays, and vertical arrows indicate the directions of change of band intensities. Spectra are displayed up to time delays of 500 ps, and both UV and visible bands decline in intensity at later times.

3.1.1 UV and Visible Absorption Band Assignments

Two-photon excitation of CCl_4 at 266 nm results in fragmentation to CCl_3 radicals and Cl-atoms, which then interact with the surrounding solvent molecules. The identities of the species that give rise to the transient UV–vis features have been the subject of prior debate,(18, 20-23) but the 330-nm feature is assigned to a charge-transfer band of Cl–CCl_4 complexes on the basis of careful arguments by Chateauneuf and further work by Crim and co-workers for related solvents.(14, 15, 17, 18) From the results of radiolysis experiments, Bühler argued that the species absorbing at 500 nm was ionic and assigned it to the ion pair $CCl_3^+\|Cl^-$, where the symbol ‖ denotes solvent separation.(20, 39) Washio et al. confirmed the spectral features in their picosecond and nanosecond pulsed radiolysis experiments and proposed that geminate recombination of CCl_3^+ and Cl^- ions produced the charge-transfer complex $CCl_3^{\delta+}$--$Cl^{\delta-}$.(23) Miyasaki et al.,(21) and more recently Zhang and Thomas,(22) observed that two-photon photolysis of CCl_4 at 266 nm gave the same broad visible absorption band as radiolysis and retained the assignment to the $CCl_3^+\|Cl^-$ ion pair.(22) In these experiments, it was recognized that the two-photon absorption at 266 nm corresponds to a total energy of 9.34 eV, which is significantly lower than the gas phase ionization energy (IE) of CCl_4 (11.47 eV(40)). This IE might be reduced in the liquid, with some reports arguing a reduction of as much as 1.5 eV.(22, 41) However, the mechanism of formation of the solvent-separated ion pair following UV excitation required some degree of speculation in the absence of spectral signatures of postulated intermediate species.

Isomeric (*iso*) forms of the parent compound have been extensively characterized in several photolysis studies of halomethanes in matrices and in liquids(24, 25, 42, 43) and shown to give rise to broad, strong visible absorption bands. A recent computational study of $CHBr_3$ isomerization showed significant charge-separation character

in *iso*-$CHBr_2$–Br, which exhibits mixed covalent and ionic character, with $(CHBr_2)^+$ Br^- contributing the major (62%) resonance structures.(26) We therefore undertook calculations of the electronic character of the *iso*-forms of CCl_4 and $CHCl_3$, following an NBO analysis similar to that reported by George et al.(26) and using the computational methods outlined in section 2.2. Figure 2 shows the derived contributions to the two isomeric forms and isomerization transition state from the principal covalent and charge-transfer resonance structures. For both *iso*-CCl_3–Cl and *iso*-$CHCl_2$–Cl, resonance structures with Cl^-–CCl_3^+ or Cl^-–$CHCl_2^+$ character constitute more than 50% of the molecular wave function. The outcomes of the TDDFT calculations for the *iso*-species are collected in Table 1 and show only modest dependence on the choice of functional. The calculations reveal very strong bands (with oscillator strengths close to 0.5) at wavelengths around 410 nm that are broadly consistent with the features we observe in Figure 1 in the visible in our time-resolved transient absorption spectra.

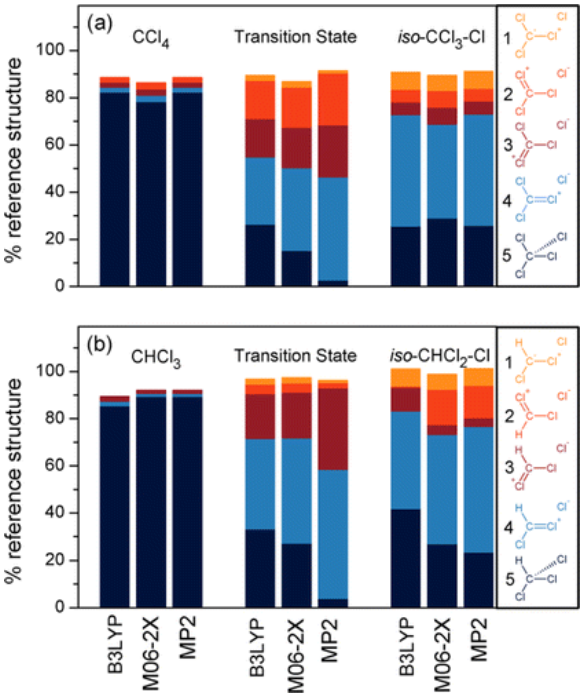

Figure 2. Principal resonance form contributions to the molecular structures of the solvent, its *iso*-form, and the transition state for their interconversion. Dark blue represents the percentage of the covalent structure, and other colors correspond to charge-separated resonance structures, which are shown for the *iso*-form at the right. Panel (a) is for CCl_4 and (b) is for $CHCl_3$. Results are shown for different computational methods described in the text.

Table 1. Calculated Wavelengths of the Electronic Absorptions of the Cl–Solvent (Cl–CCl_4 and Cl–$CHCl_3$) Complexes and *iso*-Forms (*iso*-CCl_3–Cl and *iso*-$CHCl_2$–Cl) Considered To Give Rise to the Transient UV and Visible Bands Evident in Figure 1a

		Cl–CCl_4	*iso*-CCl_3–Cl	Cl–$CHCl_3$	*iso*-$CHCl_2$–Cl
wavelength/nm	TDM06-2X	334	407	345	405
	TDCAM-B3LYP	376	420	380	414
oscillator strength	TDM06-2X	0.07	0.51	0.08	0.46
	TDCAM-B3LYP	0.11	0.49	0.13	0.44

[a]Calculations employed TDDFT methods, as described in the main text, with PCM model treatment of the solvent.

The calculations show that the ionic $CCl_3^+\|Cl^-$ that is invoked in the literature as the carrier of the visible band in photolytically or radiolytically excited CCl_4 appears to be simply an alternative description of the *iso*-CCl_3–Cl form of CCl_4.(39) For the above reasons, and because of arguments based on the time dependence of the 330-nm and 500-nm bands presented in section 3.1.2, the species giving rise to the broad absorption band at 500 nm is assigned here to *iso*-CCl_3–Cl, but it is recognized that this species exhibits significant ion pair (CCl_3^+ Cl^-) character. By analogy, and consistent with prior work,(17) the UV band in chloroform is assigned to charge transfer in Cl–$CHCl_3$ (or Cl–$CDCl_3$) complexes, and the broad visible band, to an isomeric form of chloroform, *iso*-$CHCl_2$–Cl (or *iso*-$CDCl_2$–Cl).

There is further persuasive evidence in support of the above assignments from our calculations and from other spectroscopic studies on related compounds. The computed wavelength ordering of the spectral bands for *iso*-forms and Cl–solvent complexes (Table 1) and the relative magnitudes of the oscillator strengths are consistent with the experimental observations. In particular, the very large oscillator strengths computed for the *iso*-forms, which are roughly 4–5 times larger than the Cl–solvent complex bands, are reflected in the wavelength-integrated intensities of the visible bands seen in Figure 1. The calculations do place the strong absorption bands of the *iso*-forms of CCl_4 and $CHCl_3$ to a shorter wavelength than the band centers observed experimentally, but these bands span a wide wavelength range, their exact positions are sensitive to the solvent environment and our choice of molecular geometry, and the calculations provide an incomplete description of solvation effects. Complementary to our observations, Preston et al.(44) reported similar UV (around 400 nm) and visible (centered at 450 nm) absorption bands in time-resolved electronic absorption spectra of photolyzed bromoform dissolved in CCl_4 that were assigned to the $CHBr_3$–Br complex and *iso*-$CHBr_2$–Br, respectively, on the basis of time-resolved IR spectra. The bands share an isosbestic point at 420 nm, indicating that the $CHBr_3$–Br species is the precursor of *iso*-$CHBr_2$–Br.

3.1.2 Time Dependence of the UV and Visible Bands

Our analysis of the observed time dependence of the spectral features is described in greater detail here for CCl_4 than for $CHCl_3$ (and $CDCl_3$), which follows a very similar path, but for which only the outcomes are presented. The 330-nm features for CCl_4 and $CHCl_3$ do not show pronounced evolution in their spectral shapes with time, but the visible bands shift to a shorter wavelength at early times. The shift indicates cooling of an *iso*-species that is formed internally hot. We do not attempt to fit these changing band shapes, but instead sum the intensity across 10 nm of each absorption band around each band center for every time delay. This integration gives the time-dependent intensity data shown in Figure 3. We examined the effects of integrating over much wider portions of the visible band to incorporate the early time spectral shifts, but found it made no difference to the analysis that follows. The UV band of the Cl–solvent complexes has two decay components, with the faster component being attributed to diffusive geminate recombination, while the slower loss is by either reaction or formation of the *iso*-species.(14, 15) The visible band of the isomeric form exhibits a fast rise with a time constant that appears to be similar to that for the decay of the UV band, and a much slower decay. The slow component of the visible band decays on a time scale that is comparable to the previously reported time constant of 17 ns,(18) but the decay of the UV band is much faster than the 170 ns time constant obtained in the earlier study. This discrepancy suggests two different decay processes are being observed in the two experiments that are optimized to observe kinetics on very different time scales.

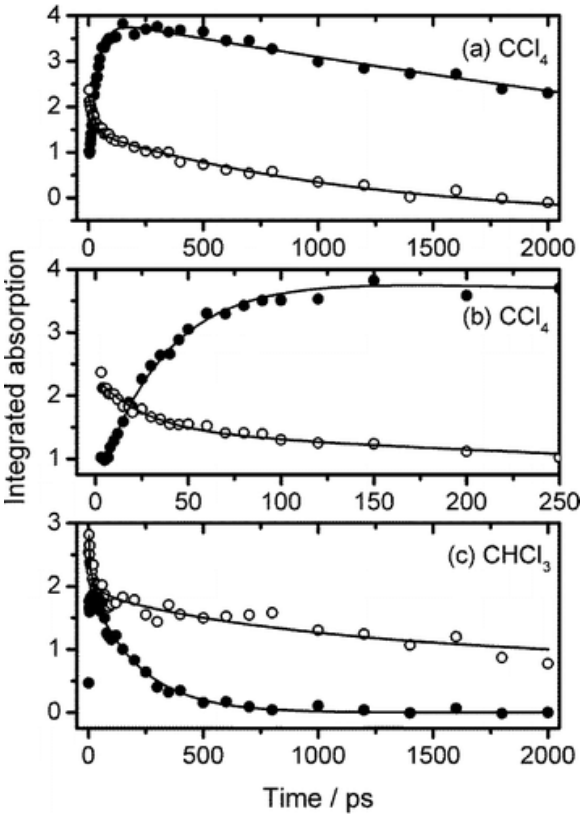

Figure 3. (a) Time dependence of the absorption centered at 330 nm (○) and 500 nm (●) observed in the transient UV–visible spectra of neat CCl_4 after excitation by a 266-nm laser pulse. The same data are shown in part (b) on an expanded time axis. Panel (c) shows corresponding data for $CHCl_3$. Absorbances have been integrated over 10-nm spectral windows. The solid lines are fits to the data as described in the text.

The time dependences of the two bands were fitted using a model based on Smoluchowski theory that was previously used by Crim and co-workers(14-16) and allows for geminate recombination of the radical photoproducts. The photoexcitation of CCl_4 is assumed to be followed by prompt dissociation to Cl + CCl_3, and the model incorporates the distance, r_0, at which the photofragment Cl and CCl_3 equilibrate in solution. As they equilibrate, the Cl-atoms can form Cl–CCl_4 complexes. The subsequent random diffusive movement of these photoproduced radical pairs is described by a relative diffusion coefficient, D_r, and CCl_3 and Cl–CCl_4 particles may recombine. The Smoluchowski model that describes the time dependence of this behavior is as follows:

(1)

$$[\mathrm{Cl}]_t = [\mathrm{Cl}]_0 \left\{1 - A erfc\left(\frac{B}{\sqrt{t}}\right)\right\} \exp(-k_1 t)$$

where $[Cl]_t$ represents the time-dependent concentration of Cl–solvent complexes, with initial value $[Cl]_0$, and the final exponential term with rate coefficient k_1 allows for reactive loss of these complexes. In eq 1, *erfc* is the complementary error function, and

(2)

$$A = \frac{R_{rec}}{r_0} \quad B = \frac{r_0 - R_{rec}}{\sqrt{4D_r}}$$

with R_{rec} as the recombination radius within which radical recombination occurs with unit efficiency. The parameter A represents the asymptotic recombination yield describing the fraction of radical pairs that recombine. Values of R_{rec} and r_0 obtained from data analysis using eq 1 are somewhat qualitative because they depend on the choice of D_r. This relative diffusion coefficient is the sum of the individual diffusion coefficients of the photofragments, $D_{Cl–CCl4}$ (for the Cl–CCl_4 complex) and D_{CCl3}, each of which is estimated using the Stokes–Einstein equation (with x denoting Cl–CCl_4 or CCl_3):

(3)

$$D_x = \frac{k_\mathrm{B}\mathrm{T}}{6\pi\eta\alpha_x}$$

Here k_B is the Boltzmann constant, T is the temperature of the solution, α_x is the radius of species x, and η is the viscosity of the solvent. The radius of a particular particle was obtained as the distance from its center of mass to the center of the furthest atom, using the Hartree–Fock 6-31G level of theory to compute geometries of Cl–CCl_4 and CCl_3. This choice of particle radius may be a slight underestimate, but we confirmed that taking the distance to the outer edge of the furthest atom (as defined by its van der Waals radius) made little difference to the outcomes of the subsequent analysis. The relative diffusion coefficient describing the recombination of a CCl_3 radical with a Cl–solvent complex was then estimated to be 2.23 $nm^2\ ns^{-1}$.

In CCl_4, we do not expect the Cl–solvent complexes to react with the solvent, suggesting that there should be no exponential decay term in eq 1 unless they are removed by another pathway. Nevertheless, this term was retained in the analysis of the data and, as will be shown, results in a very small value of k_1 consistent with our expectation. The concentration dependences in eq 1 were re-expressed in terms of transient absorption signals (S), to give the following functional form to describe the kinetics of the UV band:

(4)

$$S_t(\mathrm{UV}) = S_0(\mathrm{UV})\left\{1 - Aerfc\left(\frac{B}{\sqrt{t - t_0}}\right)\right\} \times \exp\left(-k_1(t - t_0)\right)$$

The value of the constant time offset, t_0, was fixed at 1.44 ps which corresponds to the first data point used in the analysis and is negligible compared to the 2000 ps interval over which data are fitted. As Figure 3 shows, the time dependence of the rise of the visible band appears complementary to the decay of the UV band, and we see a clear isosbestic point between the UV and visible bands in the CCl_4 spectra (Figure 1), indicating the decay of the species responsible for the 330-nm feature controls the rise of the species giving the 500-nm feature. These observations encouraged simultaneous fitting of both bands to the same parameter set, using the functional form

(5)

$$S_t(\mathrm{vis}) = S_0(\mathrm{vis})\left\{Aerfc\left(\frac{B}{\sqrt{t - t_0}}\right)\right\} \exp\left(-k_2(t - t_0)\right)$$

for the visible band. We fitted the data in Origin 8.5.1 software, using a nonlinear least-squares fitting routine with a custom functional form, and the outcomes successfully model the data, as shown by the solid lines in Figure 3. Best fit parameters and associated uncertainties are displayed in Table 2, and values of parameters A and B are similar to those reported by Sheps et al.(14) The value of A suggests that approximately 1/3 of the photofragments undergo recombination.

Table 2 also includes values for the analysis of spectra observed following $CHCl_3$ photolysis. Simultaneous fits were again performed to the time-dependent intensities of the UV and visible bands. The fits were not as robust as in case of the CCl_4 data, and so we included spectral intensities for the two corresponding bands in $CDCl_3$, with the assumption that the kinetics would be identical in the two isotopologues of chloroform. This assumption is supported by the quality of the fits. The decay of the visible band is more rapid for chloroform than for CCl_4, suggesting either reactive loss of the *iso*-chloroform species or faster isomerization back to the more energetically favorable $CHCl_3$ isomer. We return to this point later and note that this faster decay prevents an isosbestic point from developing in the spectra in Figure 1b. The greater persistence of intensity in the UV band of $CHCl_3$ compared to CCl_4 at times approaching our measurement limit points to the greater stability of the Cl–solvent complex in the former case. This deduction is supported by our calculations, as the binding energy of the Cl–$CHCl_3$ complex is roughly 50% larger than that of Cl–CCl_4 (−16 kJ mol^{-1} vs −11 kJ mol^{-1} at the M06-2X/aug-cc-pVTZ level). Computed optimized structures of these complexes are shown in the Supporting Information.

Table 2. Fit Parameters from Simultaneous Analysis of the Transient UV and Visible Bands for 266-nm Photolysis of CCl_4 and $CHCl_3$[a]

parameter	CCl_4	$CHCl_3$ and $CDCl_3$
A	0.339 ± 0.132	0.827 ± 0.068
B/$ps^{1/2}$ (/$ns^{1/2}$)	3.63 ± 0.17 (0.115 ± 0.006)	0.277 ± 0.116 (0.008 ± 0.004)
k_1/ps^{-1}	0.0003 ± 0.0003	0.0008 ± 0.0002
k_2/ps^{-1}	0.0006 ± 0.0004	0.0039 ± 0.0004

[a]Uncertainties are 1 SD from the fits.

The upper bounds of the uncertainty ranges in the values of k_1 and k_2 for CCl_4 indicate lifetimes >1 ns for the decay of the UV and visible bands, but these lifetimes are ill-determined by our measurements which extend only to 2-ns delays. However, these rate coefficients suggest that reactive losses of the Cl–CCl_4 and *iso*-CCl_3–Cl species are modest on the time scales of our experiments in neat CCl_4. The parameter B takes a similar value in CCl_4 to the value reported by Sheps et al. for CH_2Cl_2,(14, 15) but the value obtained in $CHCl_3$ (and $CDCl_3$) is anomalously low and may be an artifact of our fitting.

Washio et al. observed the decay of a spectral feature in CCl_4 at 330 nm following pulsed radiolysis of the liquid sample and measured lifetimes of ∼60 ps and ∼100 ns for two time components of the decay.(23) The latter time constant is broadly consistent with a value of 173 ns measured by Chateauneuf in UV excitation experiments,(18) but is too slow for our experiments to confirm. Zhang and Thomas photoexcited CCl_4 at 266 nm and monitored the rise of absorption at a single wavelength of 532 nm: a single-exponential fit to their data gave a time constant of 46 ps.(22) A similar analysis of the visible band growth from our measurements shown in Figure 3, which benefit from superior time resolution and signal-to-noise ratio, gives an exponential rise time constant of 37 ± 2 ps. Confining our analysis to a probe wavelength of 532 nm does not alter the derived time constant. We therefore observe the same fast spectral evolution as in these radiolysis and photolysis experiments, but we are able to monitor the decay of the UV band and the associated growth of the visible band simultaneously.

Finally in this subsection, we return to the decay rates of the visible bands in CCl_4 and $CHCl_3$. In ultrafast photolysis studies of $CHBr_3$, Tarnovsky and co-workers showed that the isomer lifetime is strongly solvent dependent,(45) being shorter in weakly interacting polar solvents than in nonpolar solvents. The origin of this effect lies in the differential solvation of the isomerization transition state compared to the isomer minimum, which lowers the effective barrier to isomerization back to the parent. Figure S2 of the Supporting Information illustrates this behavior in CCl_4 and $CHCl_3$ systems, with the outcomes of MP2/aug-cc-pVTZ intrinsic

reaction coordinate scans obtained in vacuum and in liquid solvent using the PCM method. For $CHCl_3$, the isomerization barrier from the *iso*-minimum decreases from 60 kJ mol^{-1} in vacuum to 16 kJ mol^{-1} in neat solvent. In contrast, the corresponding barrier for *iso*-CCl_3–Cl is computed to decrease from 64 to 34 kJ mol^{-1} in going from vacuum to neat solvent. These changes to barrier heights are consistent with the faster return of *iso*-$CHCl_2$–Cl to $CHCl_3$ than for the related back-isomerization in CCl_4.

3.1.3 Photochemical Reaction Scheme for CCl_4

The success of the simultaneous fit of the UV and visible bands to the same set of parameters using eqs 1 and 2 suggests that the rise of the visible band assigned to *iso*-CCl_3–Cl is a consequence of the decline in concentration of the Cl–CCl_4. A reaction scheme is proposed in Figure 4 to account for the experimental observations. Pal et al.(25) recently argued for a direct route to *iso*-bromoform via a conical intersection from the S_1 state of photoexcited $CHBr_3$, but we have no direct (experimental or theoretical) evidence for such a pathway in CCl_4 so have not included it in the scheme.

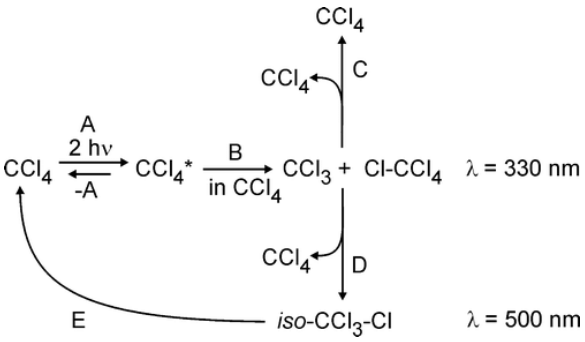

Figure 4. Chemical processes proposed to describe the production and loss of species giving rise to the absorption bands at 330 and 500 nm following UV photolysis of CCl_4. Processes A–E are described in the main text.

The mechanism in Figure 4 is initiated by step A whereby UV excitation of CCl_4 forms energized neutral CCl_4* (as also proposed by Zhang and Thomas(22)) which can either relax back to the ground state through solvent collisions, step-A, or dissociate to form CCl_3 and Cl. Promptly after the photodissociation, a fast interaction of Cl with CCl_4 forms the Cl–CCl_4 complex (step B), giving rise to the absorption band at 330 nm. The time constant for this process must be ≤2 ps to account for the fast rise observed experimentally. The proximity of a Cl-atom to a CCl_4 molecule (i.e., a loosely solvated atom) may well be sufficient to give rise to the 330-nm CT band, without the need to relax to the minimum in the potential energy surface associated with a bound Cl–CCl_4 complex. The complex subsequently has two pathways for its fast removal. The first path involves recombination of the solvated Cl-atom with CCl_3 either as a fast geminate recombination process or after diffusion, which is suggested to take hundreds of nanoseconds(18, 23, 39) and is therefore unlikely to be important on the time scale of this work. The two recombination pathways are collectively indicated as step C in Figure 4. The second path transfers the Cl-atom to a CCl_3 radical to form the metastable *iso*-CCl_3–Cl complex (step D), contributing to the growth of the absorption band at 500 nm as well as the loss of signal detected at 330 nm. This step will also be a combination of faster geminate and slower diffusive mechanisms. The conversion to the *iso*-form is consistent with the coupled kinetics reported above and the observation of an isosbestic point at approximately 400 nm in the time-dependent spectra. The subsequent decay of *iso*-CCl_3–Cl (step E) by isomerization back to CCl_4 is slow, taking nanoseconds or longer.(18, 23, 46) The decline of the absorption on the UV band to baseline within the time scale of our measurements indicates almost complete conversion of the Cl–CCl_4 complex back to two CCl_4 molecules or to *iso*-CCl_3–Cl (although we cannot discount removal of Cl–CCl_4 by reactions with impurities such as dissolved oxygen).

3.2 Photoinduced Chemistry of Alkenes and Dienes in the Chlorinated Solvents

Having established the short-time UV photochemistry of neat CCl_4 and $CHCl_3$ solvents using broad-band, time-resolved UV–vis absorption spectroscopy, the same experimental approach is applied to solutions of selected dienes and alkenes in these solvents. The unsaturated hydrocarbons provide an alternative pathway for removal of Cl–solvent complexes by chemical reaction, either by Cl-atom addition to a C═C bond or by H-atom abstraction. The *iso*-forms of the solvent molecules may also prove reactive with these added solutes.(27, 28)

3.2.1 Photoinduced Reaction of 1,5-Hexadiene in CCl_4

Our most extensive studies were carried out for addition of 1,5-hexadiene to CCl_4, and the results of these experiments are the focus of the first part of this section. Solutions of 1,5-hexadiene in CCl_4 of concentrations 0.25, 0.50, and 0.75 M were examined in the same way as for the pure solvent. Figure 5 shows examples of time-resolved transient UV–vis absorption spectra of 0.5 M 1,5-hexadiene in CCl_4.

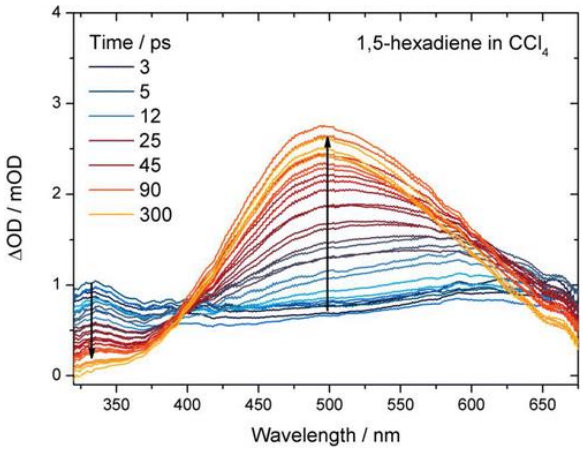

Figure 5. Transient UV–visible absorption spectra of a solution of 0.5 M 1,5-hexadiene in CCl_4 following photoexcitation at 266 nm. The inset key shows selected time delays. Spectra are plotted up to a time delay of 300 ps, and the vertical arrows indicate directions of change of the bands.

The absorption features for photoexcited solutions of 1,5-hexadiene in CCl_4 evident in Figure 5 resemble closely those observed for neat CCl_4 (Figure 1), and the time dependences of the two bands were obtained in a similar way by wavelength integration of 10-nm wide regions centered at 330 and 500 nm for each time delay. The results of this procedure are shown in Figure 6 for a 0.25 M solution of 1,5-hexadiene in CCl_4 and are contrasted with the time dependences for the neat solvent.

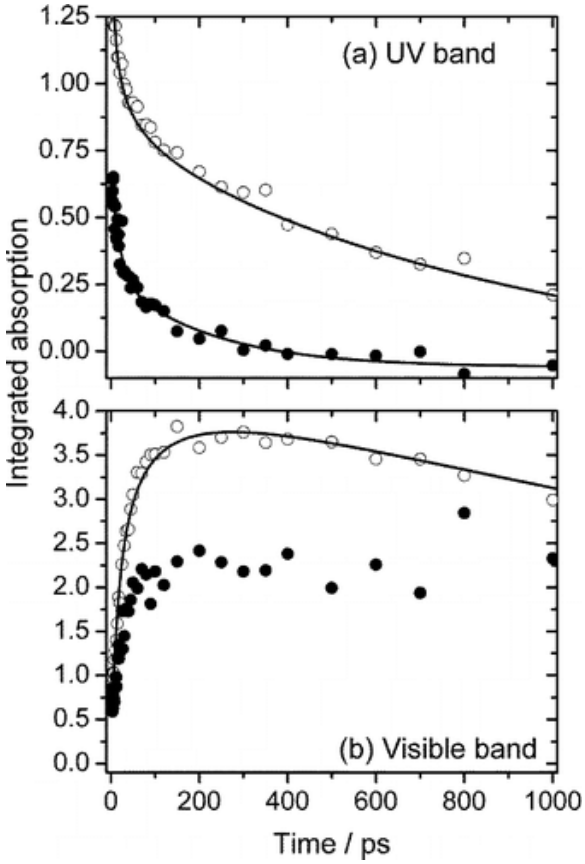

Figure 6. Time dependence of the integrated intensities of the transient (a) 330-nm and (b) 500-nm absorption bands. The panels compare a 0.25 M solution of 1,5-hexadiene in CCl_4 (●) with neat CCl_4 (○). Solid lines are fits to the data using models described in the text. The visible band data for 1,5-hexadiene solutions were not fitted in our analysis. Data were obtained in separate experimental measurements, and so absolute absorption intensities are not directly comparable.

Addition of the solute accelerates the respective decay and growth of the UV and visible bands, and the modified scheme for the solution photochemistry shown in Figure 7 accounts for these observations. In this scheme, the same processes argued to occur in neat CCl_4 are retained as steps A and B, leading to the formation of the Cl–CCl_4 complex that absorbs at 330 nm. However, the decay of the complex is now governed by the chemical reaction between the diene and the Cl–CCl_4 complex (step F) in addition to the formation of the *iso*-CCl_3–Cl species (step D, giving the absorption at 500 nm).

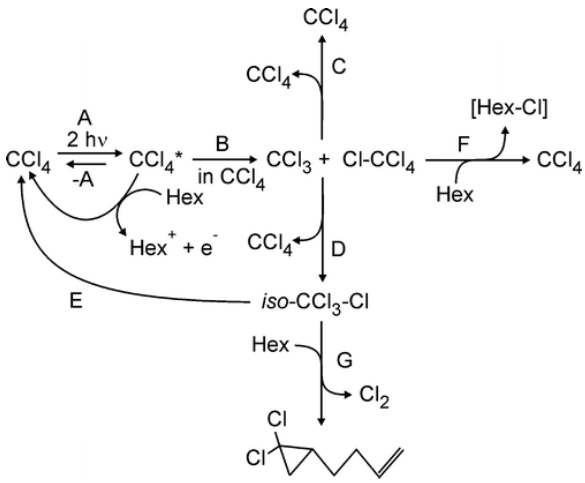

Figure 7. Chemical processes proposed to describe the kinetics of species giving rise to the absorption bands at 330 and 500 nm in UV photoexcited solutions of 1,5-hexadiene (indicated by Hex) in CCl_4. [Hex-Cl] denotes the adduct of a Cl-atom with the diene.

Calculations by Phillips and Fang suggested the *iso*-species in dichloromethane, *iso*-CH_2Cl–Cl, might act as a carbenoid.(27) Transfer of a methylene group to a C═C bond makes a cyclopropane species, with a computed energy barrier of 37 kJ mol^{-1} in the case of ethene. Step G proposes a corresponding pathway for reactive loss of *iso*-CCl_3–Cl with 1,5-hexadiene, perhaps to form a dichlorocyclopropane species by CCl_2 transfer. However, the persistence of the 500-nm band in our data to time delays of 2 ns suggests that this type of reaction is at best slow, which is consistent with the aforementioned energy barrier.

Figure 7 also incorporates formation of the radical cation of the 1,5-hexadiene, based on evidence from time-resolved IR absorption measurements(29) that is summarized in the Supporting Information. As noted earlier, the IE of CCl_4 (11.47 eV in the gas phase(40)) is substantially above the energy of two photons of the 266-nm pump laser, but the IE of 1,5-hexadiene (likely to be similar to that of 1,3-*trans*-pentadiene which is 8.70 ± 0.02 eV(47)) is lower than the energy of two-photon excited CCl_4*. We therefore suggest excitation transfer from CCl_4* to the solute causes the observed ionization of the diene. Such ionization processes have been reported previously for solutes with IEs lower than the solvent excitation energy(22) and must be fast to compete with dissociation step B. The Supporting Information contains an analysis of the time-dependent intensities of three transient IR bands centered at wavenumbers of 1260, 1350, and 1460 cm^{-1} that we assign to 1,5-hexadiene$^+$. These bands reach their maximum intensity within a few picoseconds, consistent with the proposed mechanism, but are weak which may be indicative of a minor pathway.

3.2.2 Kinetic Analysis of 1,5-Hexadiene/CCl_4 and 1,5-Hexadiene/$CHCl_3$ Photochemistry

The experimental data for the time dependence of the UV band such as those shown in Figure 6 were fitted to a model that is based on the Smoluchowski function of eq 4 for reactions in neat CCl_4 with inclusion of a factor to account for reactive loss in the 1,5-hexadiene solutions. Following Crim and co-workers, we express the time-dependent Cl–CCl_4 absorption signal in the presence of 1,5-hexadiene, S_t'(UV), as a combination of the recombination kinetics, governed by eq 4 for S_t(UV), and diffusion controlled reaction kinetics:(14-16)

(6)

$$S_t'(\mathrm{UV}) = S_t(\mathrm{UV}) \exp\left\{-4\pi R_{\mathrm{rxn}} D_{\mathrm{rxn}} C_{\mathrm{solute}} \times \left(1 + \frac{2R_{\mathrm{rxn}}}{\sqrt{\pi D_{\mathrm{rxn}}(t - t_0)}}\right)(t - t_0)\right\} + S_\infty$$

Here, R_{rxn} is the reaction radius, within which reaction between a Cl–CCl_4 complex and 1,5-hexadiene occurs with unit probability. C_{solute} denotes the concentration of the solute, which is fixed for any one experiment, D_{rxn} is the sum of diffusion constants of the reacting Cl–CCl_4 complex and diene, and S_∞ is a baseline offset evaluated at a prolonged time, which is generally found to be small. The value of D_{rxn} is fixed to a value computed from the Stokes–Einstein equation and depends only on the radii of the reactants. The parameters determining the form of S_t(UV) were obtained for the neat solvent (Section 3.1.2), and we set $k_1 = k_2 = 0$ ps^{-1} hereafter, so the only free parameters in the fits to 1,5-hexadiene/CCl_4 or 1,5-hexadiene/$CHCl_3$ data are R_{rxn} and the baseline offset.

In place of the definition of R_{rxn} given above, and by analogy to the concept of a reaction cross section, it is also instructive to consider the ratio of R_{rxn} to the sum of the molecular radii of the reactant pair as a measure of the ease of reaction. This ratio will be less than unity (i.e., not all encounters lead successfully to reaction) if the reaction is impeded by factors such as an energy barrier, steric constraints, or a transition state that is late along the reaction coordinate. We will return to this point in the later discussion.

Two sets of time-resolved UV–vis absorption spectra were recorded for each concentration of 1,5-hexadiene in CCl_4, and the UV absorption bands in all six resultant data sets were fitted simultaneously to eq 6, with appropriate choices of C_{solute}. Representative data and a fit are shown in Figure 6. The decline of the UV-band absorption to zero within 500 ps suggests the Cl–CCl_4 complexes are completely reactively removed if they do not convert to *iso*-CCl_3–Cl.

In the kinetic analysis of the diene solution data, only the time dependences of the UV bands were fitted for each solution. Table 3 lists the values of parameters derived from the fits, together with those constrained in the fitting process. The bimolecular rate coefficient for reaction of Cl–CCl_4 with 1,5-hexadiene, k_{bi}, is derived using(14)

(7)

$$k_{\mathrm{bi}} = 4\pi R_{\mathrm{rxn}} D_{\mathrm{rxn}} = (8.6 \pm 0.8) \times 10^{9}\mathrm{M}^{-1}\mathrm{s}^{-1}$$

This reaction is likely to involve adduct formation, and in time-resolved IR absorption experiments with solutions of 1,5-hexadiene in CCl_4 we were not able to observe production of HCl from either direct H-atom abstraction or an addition–elimination mechanism. The value for the bimolecular rate coefficient is similar to the k = (9.9 ± 1.3) × 10^9 M^{-1} s^{-1} reported by Chateauneuf for reaction of Cl with cyclohexene in solution in CCl_4.(18)

Table 3. Parameters Derived from Smoluchowski Model Fits to Time-Dependent UV Band Intensities for Cl–CCl_4 Complexes in Solutions of 1,5-Hexadiene, Isoprene, and 2,3-Dimethylbut-2-ene in CCl_4

	1,5-hexadiene	**isoprene**	**2,3-dimethylbut-2-ene**	***n*-pentane[a]**
D_{rxn}/nm^2 ns^{-1}	1.27	1.69	1.56	1.22
k_1/ps^{-1}	0	0	0	0
A	0.339	0.339	0.339	0.60 ± 0.04
B/ns$^{1/2}$	0.115	0.115	0.115	0.072 ± 0.025
R_{rxn}/nm	0.89 ± 0.08	0.75 ± 0.13	1.46 ± 0.09	0.83 ± 0.23
k_{bi}/M^{-1} s^{-1}	(8.6 ± 0.8) × 10^9	(9.5 ± 1.6) × 10^9	(1.7 ± 0.1) × 10^{10}	(7.7 ± 2.1) × 10^9

[a]Previous work by Sheps et al.(14) for *n*-pentane in CCl_4. A and B were constrained to values obtained from analysis of data for neat CCl_4 (see Table 1) and so uncertainties, which are not specified here, were not propagated into R_{rxn} and k_{bi} values. D_{rxn} values were computed as described in the text.

The intensities of the UV and visible bands in Figure 5 merit comparison with those in Figure 1a. We observe a decline in relative intensity of the UV band compared to the visible band in the presence of 1,5-hexadiene. The absolute absorbance of the visible band may also be smaller, and we note that Zhang and Thomas reported a reduction in the intensity of their 500-nm signal with increasing solute (cyclohexane) concentration.(22) These effects can be understood by recalling that some of the Cl–CCl_4, which generates a signal at 500 nm by decaying to *iso*-CCl_3–Cl, is now instead being consumed by the reaction. Moreover, the ionization of the solute relaxes some fraction of the CCl_4* precursor of the Cl–CCl_4. However, the absolute reduction of the absorbances upon addition of the 1,5-hexadiene must be treated with some caution for our transient spectra because conditions varied slightly between experiments with different solutions.

3.2.3 Photochemistry of Isoprene/CCl_4 and 2,3-Dimethylbut-2-ene/CCl_4 Solutions

The Smoluchowski model of eq 6 was also used to examine the decay of the 330-nm UV absorption band in solutions of 2,3-dimethylbut-2-ene (0.25, 0.50, and 0.75 M, simultaneously fitted) and isoprene (0.64 M only) in CCl_4. The parameters constrained in, and obtained from, these fits are also shown in Table 3. The fit outcomes are compared to prior results from Sheps et al.(14) for reaction of *n*-pentane in CCl_4, recalling that R_{rxn} is the key parameter derived from our fits for the reactive removal of Cl–CCl_4.

3.2.4 Comparison of Reaction Rates and Mechanisms

Isoprene and 1,5-hexadiene solutions give similar R_{rxn} values, suggesting that both proceed via related mechanisms, which we propose involve nearly diffusion limited addition of a Cl-atom across a C═C bond to form an adduct that is subsequently stabilized by solvent collisions. For a reaction of isoprene with Cl-atoms in the gas phase, >80% branching was reported for the adduct-forming channel.(10) The R_{rxn} value for *n*-pentane in CCl_4 (0.83 ± 0.23 nm)(14) is similar to those for the two dienes although reaction of this alkane must occur by H-atom abstraction, and the similarities may simply reflect nearly barrierless processes for molecules of similar size. However, the value of R_{rxn} for 2,3-dimethylbut-2-ene is larger than for the other reactions examined, despite the computed reactant-pair sizes being comparable. We previously reported time-resolved IR studies of this reaction in solution,(19) for which we observed formation of HCl(v = 0 and 1) products, indicative of direct abstraction dynamics. We argued that the steric bulk of the four $-CH_3$ groups might disfavor Cl-atom addition to the central C═C bond in this solute, with the support of evidence from gas-phase studies with systematic variation of the substitution around the C═C bond.(4) The larger R_{rxn} value is consistent with this argument because it indicates a barrierless abstraction reaction at the periphery of the molecule. The value of k_{bi} for the 2,3-dimethylbut-2-ene reaction agrees within uncertainties with a prior report by Chateauneuf of $(1.2 \pm 0.7) \times 10^{10}$ M^{-1} s^{-1}.(18)

Contrary to the observations for 2,3-dimethylbut-2-ene, photochemical studies of both 1,5-hexadiene and isoprene solutions in CCl_4 using transient IR absorption spectroscopy showed no measurable HCl production.(29) 2,3-dimethylbut-2-ene has 12 equivalent H-atoms, and abstraction of any one of them creates an allylic radical with resonance-stabilized forms. 1,5-hexadiene and isoprene only have four and three such labile H-atoms, respectively. Abstraction of the remaining vinylic H-atoms by a Cl-atom is considerably less energetically favorable. For *n*-pentane there are also 12 H-atoms accessible to an attacking Cl-atom, and we and others have observed HCl production,(14, 19) but the formation of a primary or secondary alkyl radical coproduct by H-abstraction is significantly less exothermic than formation of an allylic radical. Hence, the transition state for abstraction is likely to be later along the reaction coordinate for *n*-pentane, which may account for the smaller value of R_{rxn}.

Values of the fit parameters obtained for photochemical reactions of 1,5-hexadiene and isoprene in the two different solvents $CHCl_3$ and in CCl_4 are compared in Table 4. The viscosity of chloroform is lower than that of CCl_4, giving larger diffusion coefficients for the former solvent. The smaller values of R_{rxn} for reactions of 1,5-hexadiene and isoprene in $CHCl_3$ than in CCl_4 may indicate later or higher (but nevertheless modest) barriers to reaction than for the equivalent process in CCl_4, perhaps because of the greater stability or lower reactivity of the Cl–$CHCl_3$ complex than the analogous species in CCl_4 solution. Our computed binding energies at the M06-2X/aug-cc-pVTZ level for these two complexes support these suggestions: respective values for Cl–CCl_4 and Cl–$CHCl_3$ are −16 and −11 kJ mol^{-1}. In a similar vein, Sheps et al. previously proposed that the Cl–CCl_4 complex was more reactive with *n*-pentane than the corresponding Cl–CH_2Cl_2 species invoked for reactions in dichloromethane,(15) and Chateauneuf reported a significantly faster activation-controlled reaction of Cl–solvent complexes with CH_2Cl_2 in solution in CCl_4 than in neat CH_2Cl_2.(11) The smaller disparity between the bimolecular rate coefficients listed in Table 4 than between R_{rxn} values for the two solvents is a result of compensation from the lower viscosity, and hence faster diffusion, in $CHCl_3$.

Table 4. Comparison of the Values Obtained from Smoluchowski Model Fits to the Time-Dependent UV Band Intensities of Cl–Solvent Complexes in Solutions of 1,5-Hexadiene and Isoprene in $CHCl_3$ and CCl_4a

	1,5-hexadiene/$CHCl_3$	**1,5-hexadiene/CCl_4**	**isoprene/$CHCl_3$**	**isoprene/CCl_4**
D_{rxn}/nm^2 ns^{-1}	2.31	1.27	3.05	1.69
k_1/ps^{-1}	0	0	0	0
A	0.828	0.339	0.828	0.339

B/ns$^{1/2}$	0.0087	0.115	0.0087	0.115
R_{rxn}/nm	0.28 ± 0.14	0.89 ± 0.08	0.56 ± 0.16	0.75 ± 0.13
k_{bi}/M^{-1} s^{-1}	(4.9 ± 2.5) × 10^9	(8.6 ± 0.8) × 10^9	(1.3 ± 0.4) × 10^{10}	(9.5 ± 1.6) × 10^9

[a]A and B were constrained to values derived from neat solvents, and D_{rxn} was calculated as described in the main text. All other parameters were derived from fits to data for 0.5 M solutions.

4 Conclusions

Transient absorption spectra were obtained with picosecond time resolution in the near-UV and visible regions following UV photoexcitation of liquid samples of CCl_4, $CHCl_3$, and solutions of 1,5-hexadiene, isoprene, and 2,3-dimethylbut-2-ene in these chlorinated solvents. The transient absorption spectra show bands centered around 330 and 500 nm in both CCl_4 and $CHCl_3$ that have been reported previously in both two-photon UV excitation and pulsed radiolysis experiments. The assignment of the UV band to charge transfer within a Cl–solvent complex is well established, but the carrier of the visible band has been the subject of some debate. In CCl_4, we assign the visible band to *iso*-CCl_3–Cl based on evidence from the time dependence of the absorption (which grows on a time scale commensurate with the decay of the UV band intensity), TDDFT calculations, and analogous studies in other halogenated solvents. Electronic structure calculations show the *iso*-CCl_3–Cl has >50% charge-separated resonance character, so our assignment is similar in spirit to previous attributions to either a solvent separated ion pair ($CCl_3^+ \| Cl^-$)(20, 39) or a charge-transfer complex ($CCl_3^{\delta+}$–$Cl^{\delta-}$) resulting from the geminate recombination of CCl_3^+ and Cl^- ions.(23) However, our proposed mechanism for formation of the *iso*-CCl_3–Cl by recombination of neutral, solvated Cl and CCl_3 does not involve separated-ion recombination pathways. Analogous assignments are proposed for the carriers of the corresponding UV and visible bands observed in photoexcited chloroform. The time dependences of the bands were analyzed using a model based on Smoluchowski theory, which also incorporates geminate recombination.

Addition of an unsaturated organic solute (1,5-hexadiene, isoprene, or 2,3-dimethylbut-2-ene) provides alternative reactive pathways for removal of the Cl–solvent complex, and so the decay of the UV band becomes faster. The dominant reaction pathway involves Cl–adduct formation, with the exception of 2,3-dimethylbut-2-ene for which a direct abstraction pathway to form HCl competes effectively. Our interpretation of the mechanism for HCl production from our earlier transient IR-absorption study(19) is reinforced by the current data analysis: a significantly larger reaction radius for Cl-atom reaction with 2,3-dimethylbut-2-ene than for 1,5-hexadiene or isoprene is consistent with a barrierless abstraction reaction at the periphery of the $(CH_3)_2C{=}C(CH_3)_2$ molecule.

Bimolecular rate coefficients for the reactions of Cl-atoms with 1,5-hexadiene, isoprene, and 2,3-dimethylbut-2-ene in solution in CCl_4 at 294 K are, respectively, (8.6 ± 0.8) × 10^9, (9.5 ± 1.6) × 10^9, and (1.7 ± 0.1) × 10^{10} M^{-1} s^{-1}, with the latter agreeing within uncertainties with a prior determination by Chateauneuf.(18) The Cl–Cl_4 complex in CCl_4 solutions has a lower binding energy and, hence, is more reactive toward 1,5-hexadiene than the corresponding complex, Cl–$CHCl_3$, when $CHCl_3$ is used as the solvent. A further channel is observed by time-resolved IR spectroscopy that involves ionization of the organic solutes by energy transfer from photoexcited CCl_4*. However, we do not observe a possible pathway for removal of *iso*-CCl_3–Cl by addition of CCl_2 across a C=C bond in the 1,5-hexadiene on the time scale of our measurements.

Supporting Information

Supporting Information describes the computed structures of the Cl–solvent complexes and the energetics of the isomerization pathways from CCl_4 to *iso*-CCl_3–Cl and from $CHCl_3$ to *iso*-$CHCl_2$–Cl. Analysis is reported of the transient infrared absorption bands observed following UV photoexcitation of 1,5-hexadiene solutions in CCl_4 and $CDCl_3$. This material is available free of charge via the Internet at http://pubs.acs.org.

Terms & Conditions

Acknowledgment

The Bristol group gratefully acknowledges financial support from the EPSRC (Programme Grant EP/G00224X) and the ERC (Advanced Grant 290966 CAPRI). Experimental measurements were conducted at the ULTRA Laser Facility which is supported by STFC (Facility Grant ST/501784). S.A.R. acknowledges financial support from the NSF (CHE-1057951).

References

1 Murray, C.; Orr-Ewing, A. J. The Dynamics of Chlorine Atom Reactions with Polyatomic Organic Molecules Int. Rev. Phys. Chem. **2004**, 23, 435– 482

2 Murray, C.; Pearce, J. K.; Rudic, S.; Retail, B.; Orr-Ewing, A. J. Stereodynamics of Chlorine Atom Reactions with Organic Molecules J. Phys. Chem. A **2005**, 109, 11093– 11102

3 Pilgrim, J. S.; Taatjes, C. A. Infrared Absorption Probing of the $Cl+C_3H_6$ Reaction: Rate coefficient for HCl Production Between 290 and 800 K J. Phys. Chem. A **1997**, 101, 5776– 5782

4 Ezell, M. J.; Wang, W.; Ezell, A. A.; Soskin, G.; Finlayson-Pitts, B. J. Kinetics of Reactions of Chlorine Atoms with a Series of Alkenes at 1 atm and 298 K: Structure and Reactivity Phys. Chem. Chem. Phys. **2002**, 4, 5813– 5820

5 Coquet, S.; Ariya, P. A. Kinetics of the Gas-Phase Reactions of Cl Atom with Selected C-2-C-5 Unsaturated Hydrocarbons at $283 < T < 323$ K Int. J. Chem. Kinet. **2000**, 32, 478– 484

6 Sharma, A.; Pushpa, K. K.; Dhanya, S.; Naik, P. D.; Bajaj, P. N. Rate Coefficients and Products for Gas-Phase Reactions of Chlorine Atoms with Cyclic Unsaturated Hydrocarbons at 298 K Int. J. Chem. Kinet. **2010**, 42, 98– 105

7 Sharma, A.; Pushpa, K. K.; Dhanya, S.; Naik, P. D.; Bajaj, P. N. Rate Constants for the Gas-Phase Reactions of Chlorine Atoms with 1,4-Cyclohexadiene and 1,5-Cyclooctadiene at 298 K Int. J. Chem. Kinet. **2011**, 43, 431– 440

8 Stutz, J.; Ezell, M. J.; Ezell, A. A.; Finlayson-Pitts, B. J. Rate Constants and Kinetic Isotope Effects in the Reactions of Atomic Chlorine with n-Butane and Simple Alkenes at Room Temperature J. Phys. Chem. A **1998**, 102, 8510– 8519

9 Estillore, A. D.; Visger, L. M.; Suits, A. G. Imaging the Dynamics of Chlorine Atom Reactions with Alkenes J. Chem. Phys. **2010**, 133, 074306

10 Suh, I.; Zhang, R. Kinetic Studies of Isoprene Reactions Initiated by Chlorine Atom J. Phys. Chem. A **2000**, 104, 6590– 6596

11 Chateauneuf, J. Kinetic Evidence for Chlorine Atom Complexes in “Noncomplexing” Solvents J. Org. Chem. **1999**, 64, 1054– 1055

12 Dneprovskii, A. S.; Kuznetsov, D. V.; Eliseenkov, E. V.; Fletcher, B.; Tanko, J. M. Free Radical Chlorinations in Halogenated Solvents: Are there any Solvents which are Truly Noncomplexing? J. Org. Chem. **1998**, 63, 8860

13 Raftery, D.; Iannone, M.; Phillips, C. M.; Hochstrasser, R. M. Hydrogen Abstraction Dynamics in Solution Studied by Picosecond Infrared-Spectroscopy Chem. Phys. Lett. **1993**, 201, 513– 520

14 Sheps, L.; Crowther, A. C.; Carrier, S. L.; Crim, F. F. Time-Resolved Spectroscopic Study of the Reaction Cl + n-C_5H_{12} → HCl + C_5H_{11} in Solution J. Phys. Chem. A **2006**, 110, 3087– 3092
15 Sheps, L.; Crowther, A. C.; Elles, C. G.; Crim, F. F. Recombination Dynamics and Hydrogen Abstraction Reactions of Chlorine Radicals in Solution J. Phys. Chem. A **2005**, 109, 4296– 4302
16 Elles, C. G.; Cox, M. J.; Barnes, G. L.; Crim, F. F. Recombination and Reaction Dynamics Following Photodissociation of CH_3OCl in Solution J. Phys. Chem. A **2004**, 108, 10973– 10979
17 Chateauneuf, J. E. Charge-Transfer Absorption Spectra of Chlorine Atoms in Halogenated Solvents Chem. Phys. Lett. **1989**, 164, 577– 580
18 Chateauneuf, J. E. Direct Measurement of the Absolute Kinetics of Chlorine Atom in CCl_4 J. Am. Chem. Soc. **1990**, 112, 442– 444
19 Abou-Chahine, F.; Greaves, S. J.; Dunning, G. T.; Orr-Ewing, A. J.; Greetham, G. M.; Clark, I. P.; Towrie, M. Vibrationally Resolved Dynamics of the Reaction of Cl Atoms with 2,3-dimethylbut-2-ene in Chlorinated Solvents Chem. Sci. **2013**, 4, 226– 237
20 Bühler, R. E. The Cations of CCl_4 in Non-Polar Liquid Systems Radiat. Phys. Chem. **1983**, 21, 139– 146
21 Miyasaka, H.; Masuhara, H.; Mataga, N. Picosecond 266-nm Multiphoton Laser Photolysis of Liquid Alkyl Chlorides - Production of Ionic Species Chem. Phys. Lett. **1985**, 118, 459– 463
22 Zhang, G.; Thomas, J. K. The Laser Two-Photon Photolysis of Liquid Carbon Tetrachloride Photochem. Photobiol. **2006**, 82, 158– 162
23 Washio, M.; Yoshida, Y.; Hayashi, N.; Kobayashi, H.; Tagawa, S.; Tabata, Y. Study of Radiation-Induced Reaction in Liquid Carbon-Tetrachloride by means of Picosecond Pulse-Radiolysis Radiat. Phys. Chem. **1989**, 34, 115– 120
24 Preston, T. J.; Shaloski, M. A.; Crim, F. F. Probing the Photoisomerization of $CHBr_3$ and CHI_3 in Solution with Transient Vibrational and Electronic Spectroscopy J. Phys. Chem. A **2013**, 117, 2899– 2907
25 Pal, S. K.; Mereshchenko, A. S.; Butaeva, E. V.; El-Khoury, P. Z.; Tarnovsky, A. N. Global Sampling of the Photochemical Reaction Paths of Bromoform by Ultrafast Deep-UV Through Near-IR Transient Absorption and Ab Initio Multiconfigurational Calculations J. Chem. Phys. **2013**, 138, 124501
26 George, L.; Kalume, A.; Esselman, B. J.; Wagner, J.; McMahon, R. J.; Reid, S. A. Spectroscopic and Computational Studies of Matrix-Isolated Iso-$CHBr_3$: Structure, Properties, and Photochemistry of Iso-Bromoform J. Chem. Phys. **2011**, 135, 124503
27 Phillips, D. L.; Fang, W.-H. Density Functional Theory Investigation of the Reactions of Isodihalomethanes (CH_2X–X where X = Cl, Br, or I) with Ethylene: Substituent Effects on the Carbenoid Behavior of the CH_2X–X Species J. Org. Chem. **2001**, 66, 5890– 5896
28 Phillips, D. L.; Fang, W.-H.; Zheng, W.-H. Isodiiodomethane is the Methylene Transfer Agent in Cyclopropanation Reactions with Olefins using Ultraviolet Photolysis of Diiodomethane in Solutions: A Density Functional Theory Investigation of the Reactions of Isodiiodomethane, Iodomethyl Radical, and Iodomethyl Cation with Ethylene J. Am. Chem. Soc. **2001**, 123, 4197– 4203
29 Abou-Chahine, F.Chemical Reaction Dynamics in Solution in Chlorinated Solvents. Ph.D. Thesis, University of Bristol, 2013.
30 Greetham, G. M.; Burgos, P.; Cao, Q.; Clark, I. P.; Codd, P. S.; Farrow, R. C.; George, M. W.; Kogimtzis, M.; Matousek, P.; Parker, A. W.ULTRA: A Unique Instrument for Time-Resolved Spectroscopy Appl. Spectrosc. **2010**, 64, 1311– 1319
31 Frisch, M. J.; Trucks, G. W.; Schlegel, H. B.; Scuseria, G. E.; Robb, M. A.; Cheeseman, J. R.; Scalmani, G.; Barone, V.; Mennucci, B.; Petersson, G. A.; Gaussian 09; Gaussian Inc.: Wallingford, CT, 2009.
32 Zhao, Y.; Truhlar, D. G. The M06 Suite of Density Functionals for Main Group Thermochemistry, Thermochemical Kinetics, Noncovalent Interactions, Excited States, and Transition Elements: Two New Functionals and Systematic Testing of Four M06-Class Functionals and 12 other Functionals Theor. Chem. Acc. **2008**, 120, 215– 241
33 Glendening, E. D.; Weinhold, F. Natural Resonance Theory: I. General Formalism J. Comput. Chem. **1998**, 19, 593– 609

34 Glendening, E. D.; Weinhold, F. Natural Resonance Theory: II. Natural Bond Order and Valency J. Comput. Chem. **1998**, 19, 610– 627
35 Glendening, E. D.; Badenhoop, J. K.; Reed, A. E.; Carpenter, J. E.; Bohmann, J. A.; Morales, C. M.; Weinhold, F. NBO 5.9; Theoretical Chemistry Institute, University of Wisconsin-Madison, Madison, 2004.
36 Yanai, T.; Tew, D. P.; Handy, N. C. A New Hybrid Exchange-Correlation Functional using the Coulomb-Attenuating Method (CAM-B3LYP) Chem. Phys. Lett. **2004**, 393, 51– 57
37 Peach, M. J. G.; Helgaker, T.; Salek, P.; Keal, T. W.; Lutnaes, O. B.; Tozer, D. J.; Handy, N. C. Assessment of a Coulomb-Attenuated Exchange-Correlation Energy Functional Phys. Chem. Chem. Phys. **2006**, 8, 558– 562
38 Mardirossian, N.; Parkhill, J. A.; Head-Gordon, M. Benchmark Results for Empirical Post-GGA Functionals: Difficult Exchange Problems and Independent Tests Phys. Chem. Chem. Phys. **2011**, 13, 19325– 19337
39 Bühler, R. E.; Hurni, B. Transient Ion-Pair ($CCl_3^+.Cl^-$) in Irradiated Liquid CCl_4 - Evidence for a Delayed Geminate Ion Neutralization Helv. Chim. Acta **1978**, 61, 90– 96
40 NIST ChemistryWebbook, NIST Standard Reference Database Number 69 In National Institute of Standards and Technology; Linstrom, P. J.; Mallard, W. G., Eds.; Gaithersburg, MD 20899.
41 Takayanagi, T.; Kurosaki, Y.; Tachikawa, H. Ab Initio MO Calculations on Potential Energy Surfaces of CCl_4, is a C_{2v} Contact Ion Pair an Isomer of T_d-CCl_4? Radiat. Phys. Chem. **1999**, 55, 367– 371
42 Tarnovsky, A. N.; Pascher, I.; Pascher, T. Reactivity of Iso-Diiodomethane and Iso-Iodoform, Isomers of CH_2I_2 and CHI_3, Toward the Double Bond of a Variety of Cycloalkenes J. Phys. Chem. A **2007**, 111, 11814– 11817
43 El-Khoury, P. Z.; Kwok, W. M.; Guan, X.; Ma, C.; Phillips, D. L.; Tarnovsky, A. N. Photochemistry of Iodoform in Methanol: Formation and Fate of the Iso-CHI_2-I Photoproduct ChemPhysChem **2009**, 10, 1895– 1900
44 Preston, T. J.; Dutta, M.; Esselman, B. J.; Kalume, A.; George, L.; McMahon, R. J.; Reid, S. A.; Crim, F. F. Formation and Relaxation Dynamics of Iso-CH_2Cl-I in Cryogenic Matrices J. Chem. Phys. **2011**, 135, 114503– 114510
45 El-Khoury, P. Z.; Pal, S. K.; Mereshchenko, A. S.; Tarnovsky, A. N. The Formation and Back Isomerization of Iso-H_2C-Br-Br on a 100-ps Time Scale Following 255-nm Excitation of CH_2Br_2 in Acetonitrile Chem. Phys. Lett. **2010**, 493, 61– 66
46 Bühler, R. E. The Cations of CCl_4 in Non-Polar Liquid Systems Radiat. Phys. Chem. **1983**, 21, 139– 146
47 Franklin, J. L.; Mogenis, A. An Electron Impact Study of Ions from Several Dienes J. Phys. Chem. **1967**, 71, 2820– 2824